*Protein Science* (1999), *8*:50–64. Cambridge University Press. Printed in the USA.


# Protein–protein recognition: An experimental and computational study of the R89K mutation in Raf and its effect on Ras binding

JUN ZENG,[1] MASHA FRIDMAN,[2] HIROSHI MARUTA,[2] HERBERT R. TREUTLEIN,[2] AND THOMAS SIMONSON[1]

[1]Laboratoire de Biologie Structurale (C.N.R.S.), I.G.B.M.C., 1 rue Laurent Fries, 67404 Illkirch (C.U. de Strasbourg), France
[2]Ludwig Institute for Cancer Research, P.O. Royal Melbourne Hospital, Melbourne, Victoria 3050, Australia

(RECEIVED April 24, 1998; ACCEPTED August 25, 1998)

**Abstract**

Binding of the protein Raf to the active form of Ras promotes activation of the MAP kinase signaling pathway, triggering cell growth and differentiation. Raf/Arg89 in the center of the binding interface plays an important role determining Ras–Raf binding affinity. We have investigated experimentally and computationally the Raf-R89K mutation, which abolishes signaling in vivo. The binding to [$\gamma$-$^{35}$S]GTP-Ras of a fusion protein between the Raf-binding domain (RBD) of Raf and GST was reduced at least 175-fold by the mutation, corresponding to a standard binding free energy decrease of at least 3.0 kcal/mol. To compute this free energy and obtain insights into the microscopic interactions favoring binding, we performed alchemical simulations of the RBD, both complexed to Ras and free in solution, in which residue 89 is gradually mutated from Arg into Lys. The simulations give a standard binding free energy decrease of 2.9 $\pm$ 1.9 kcal/mol, in agreement with experiment. The use of numerous runs with three different force fields allows insights into the sources of uncertainty in the free energy and its components. The binding decreases partly because of a 7 kcal/mol higher cost to desolvate Lys upon binding, compared to Arg, due to better solvent interactions with the more concentrated Lys charge in the unbound state. This effect is expected to be general, contributing to the lower propensity of Lys to participate in protein–protein interfaces. Large contributions to the free energy change also arise from electrostatic interactions with groups up to 8 Å away, namely residues 37–41 in the conserved effector domain of Ras (including 4 kcal/mol from Ser39 which loses a bifurcated hydrogen bond to Arg89), the conserved Lys84 and Lys87 of Raf, and 2–3 specific water molecules. This analysis will provide insights into the large experimental database of Ras–Raf mutations.

**Keywords:** protein; molecular recognition; signal transduction

Protein–protein interactions regulate much of the information flow along signal transduction pathways within cells. Specificity of recognition is critical for maintaining the integrity of the signal. An important example is the recognition between Ras and Raf. Members of the Ras superfamily of small GTP-binding proteins regulate many cellular functions, including control of protein transport, cytoskeletal regulation, and cell growth (McCormick & Wittinghofer, 1996). Ras itself activates several signaling pathways, and oncogenic mutants of Ras are detected in many human cancers. Raf-1 is one of the immediate downstream targets of Ras, promoting Ras-dependent activation of the MAP kinase pathway (Heidecker et al., 1992; Moodie et al., 1993; Zhang et al., 1993), which triggers cell growth and differentiation. Interactions of Raf with Ras are mediated by two domains of Raf, including the so-called "Ras-binding domain" (RBD) in the N-terminus of Raf, which binds directly to the GTP-bound form of Ras (Vojtek et al., 1993; Emerson et al., 1995). Ras in its GDP-bound, or "off" form does not bind to Raf. Mutations of several residues in this domain of Raf have been shown to disrupt Ras–Raf binding and consequently Raf activation (Zhang et al., 1993; Shirouzu et al., 1994; Nassar et al., 1995; Block et al., 1996). A detailed understanding of Ras–RBD interactions will thus be of value in the design of antagonists of Raf, with potential therapeutic applications. It will also help to understand the recognition of other Ras targets, such as Ral guanine-nucleotide exchange factor, whose RBD has a structure very similar to that of Raf-RBD (Geyer et al., 1997; Huang et al., 1997) and which couples Ras to the Rho/Rac cytoskeletal regulation pathway.

Reprint requests to: Thomas Simonson, Laboratoire de Biologie Structurale (C.N.R.S.), I.G.B.M.C., 1 rue Laurent Fries, 67404 Illkirch (C.U. de Strasbourg), France; e-mail: simonson@igbmc.u-strasbg.fr.

*Abbreviations:* RBD, Ras-binding domain; RRH, Ras recognition helix; H, helix conformation; T, turn conformation; GST, glutathione S-transferase; MAP, mitogen-activated protein; BSA, bovine serum albumin; NMR, nuclear magnetic resonance; RMSD, RMS deviation; RMSF, RMS fluctuation.

Here, we investigate the effect of the R89K mutation in the RBD upon the Ras–RBD binding affinity, both experimentally and computationally. Arg89 has been shown by in vitro and in vivo mutagenesis to be important for Ras–Raf recognition (Zhang et al., 1993; Shirouzu et al., 1994; Nassar et al., 1995; Block et al., 1996). The residue equivalent to Arg89 in the structural homologue Ral guanine-nucleotide exchange factor is in fact a lysine. While the R89K mutation preserves the net electrostatic charge, it reduces the binding constant by a factor of more than 175 (see below), corresponding to a decrease in standard binding free energy of more than 3.0 kcal/mol, effectively abolishing Ras-dependent activation of Raf. The calculations below suggest a plausible mechanism for this decrease.

The simulations also provide general insights into protein–protein binding. Arginine residues have the highest propensity of all 20 amino acids to be present in protein–protein interfaces, where they participate in over one-third of all hydrogen bonds (Janin et al., 1988). The thermodynamics of protein–protein binding involves many competing factors (Janin, 1995), which free energy simulations can help unravel, as they provide a direct link between the microscopic structure and the binding free energy (Gao et al., 1989; Miyamoto & Kollman, 1993; Pomes et al., 1995). Free energy simulations require very extensive conformational sampling (Tobias et al., 1989; Hermans et al., 1992; Wade & McCammon, 1992; Hodel et al., 1993, 1995). Therefore, a systematic analysis of stable RBD conformations was carried out earlier (Zeng et al., 1998), and numerous long runs were performed here. The molecular mechanics force field employed can also be a source of systematic error, and so we report free energy simulations done with three different force fields.

A complication related to the multiple minima problem arises in the present system because in the NMR structure of the free RBD, the Arg89 region occupies a mixture of two conformations (Emerson et al., 1995). In one, the Ras-recognition helix (RRH, residues 78–89) extends all the way to Arg89; we refer to this as the "helical," or H conformation. In the other, the helix is broken after residue 87, and 87–90 form a reverse turn; we refer to this as the "turn," or T conformation. Only the H conformation appears to be populated in the complex (Nassar et al., 1995; Zeng et al., 1999). Thus, an induced ordering occurs upon binding. Its free energy cost is expected to differ for the native and mutant proteins, and this was confirmed by extensive free energy simulations (Zeng et al., 1998): the R89K mutation destabilizes the H conformation by about 0.5–0.6 kcal/mol relative to the T conformation. This is significant compared to the experimental reduction in binding free energy produced by the mutation. Therefore, to correctly compute the binding free energy change due to the mutation, this ordering must be viewed as an integral part of the binding process, as shown in the thermodynamic cycle I of Figure 1.

Another difficulty arises because the exact Ras–RBD structure is not known experimentally. However, as shown below, the extremely high overall sequence and structural homology between Ras and the protein Rap allow the Ras–RBD complex to be modeled with confidence by superimposing the experimental Ras structure (deVos et al., 1988; Pai et al., 1989; Kraulis et al., 1994) on the Rap moiety in the Rap–RBD crystal complex (Nassar et al., 1995; Nassar et al., 1996).

This paper is organized as follows. The next section describes Results. The experimental results are described, followed by the simulations of the native and mutant RBD in solution, and of the complexes between Ras and the native and mutant RBD. More extensive simulations of the native complex using a larger model will be reported elsewhere (Zeng et al., 1999). Next, the Arg89 → Lys free energy calculations in the free RBD and the Ras–RBD complex are described. The following section is a Discussion. Materials and methods are described last.

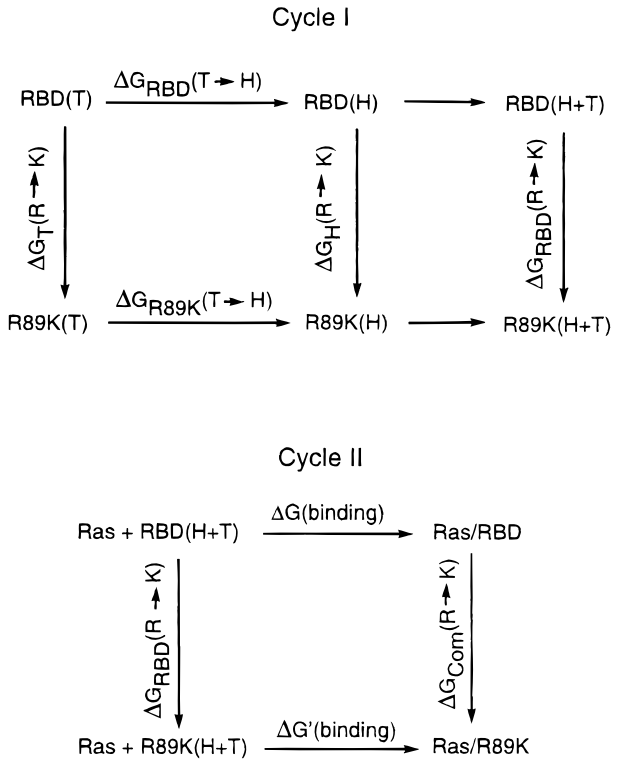


**Fig. 1.** Thermodynamic cycles connecting the free and complexed states of the native and mutant RBD. Cycle I connects the H and T conformations of the free RBD (native and R89K mutant), as well as the H + T state, which represents the equilibrium mixture of H and T states in solution. Cycle II connects the H + T states of the free RBD (native and mutant) with the complexed states. Free energy changes discussed in the text are indicated along each leg of the cycles.

## Results

### *Experimental effect of the mutation on binding*

Figure 2A shows 15% SDS-PAGE of purified GST, GST-RBD wild-type, Leu89 and Lys89 proteins. The gel used to measure GST and GST-RBD protein concentrations by densitometry is shown in Figure 2B. The constructs were diluted in binding buffer that contained 0.5 mg/mL bovine serum albumin (BSA), which appears as a prominent band at the top of the gel. GST and the Leu89 mutant were used as negative controls in the binding assay. The Leu89 mutant was shown earlier to adopt a native-like fold (Block et al., 1996), and to disrupt the Ras–Raf-1 interaction both in vivo and in vitro (Fabian et al., 1994; Block et al., 1996). The R89K mutant RBD is assumed to be even more native-like, and thus folded. It is equally inactive: the radioactivity measured (Table 1) was around 0.6 ± 0.1%, or 1/175 of that associated with wild-type RBD, comparable to the nonspecific binding measured in the absence of the RBD. The precision of the experiments does not

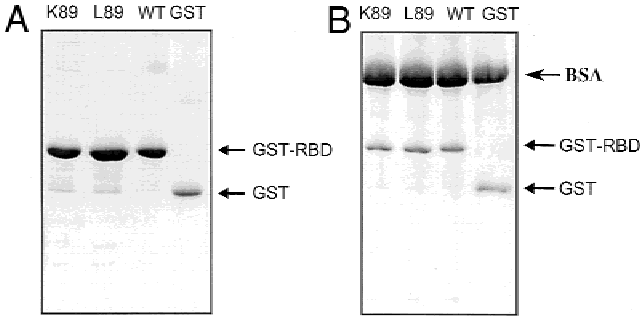


**Fig. 2.** In vitro binding between Ras-GTP-$\gamma$-S$^{35}$ and GST-RBD constructs. **A:** 15% SDS-PAGE of purified constructs. **B:** 15% SDS-PAGE used in densitometry. The amounts of each protein were estimated as follows: 15.0 $\mu$g of BSA, 3.1 $\mu$g of GST, 2.6 $\mu$g of wild-type, 2.8 $\mu$g of L89, and 2.6 $\mu$g of K89 GST-RBD. Aliquots of the same solutions were used in the binding assay.

permit a separation of specific and nonspecific binding at this level of accuracy, and so the weak observed binding only provides an upper bound for specific binding. The reduction in binding corresponds to a standard binding free energy decrease of 3.0 kcal/mol or more for the R89K mutant.

The possibility exists that the R89K mutant may bind Ras in a different way, or even with a different stoichiometry than the native RBD. While this seems unlikely, it would in any case only lower further the binding free energy for the native-like mode of binding assumed in the calculations.

### *Building the Ras–RBD complex*

The structure of Ras has been determined by both crystallography and NMR (deVos et al., 1988; Pai et al., 1989; Kraulis et al., 1994), and the structure of the RBD of human Raf-1 has been determined both in solution (Emerson et al., 1995), and in a crystal complex with the protein Rap1A, a protein with very high sequence homology to Ras (Nassar et al., 1995; Nassar et al., 1996). An (E30D,K31E) double mutant of Rap, known as "Raps," was also solved in complex with the RBD (Nassar et al., 1996). This double mutation restores two residues present in Ras but not in Rap, which are known to be important for specificity of Raf binding. The sequences of Ras and Raps have 57% identity and 90% similarity; they are identical in the interface region except for the I27H mutation (Fig. 3A), and there are only two single-residue gaps in Ras, far from the RBD interface. In the crystal structures, almost all the direct Rap–Raf or Raps–Raf interactions involve the highly conserved effector domain of Rap (residues 32–40), whose sequence is identical to that in Ras, and which forms a tight network of electrostatic interactions with Raf. The structure of Raps in the crystal complex agrees with the crystal structure of Ras within 0.81 Å (backbone RMS deviation (RMSD)). For the region surrounding Arg89, which is at the center of the interface, the RMSD is only 0.29 Å (residues within 8 Å of Arg89). The two structures are compared in Figure 3B. Because the backbone structure is so highly conserved and the sequence of side chains in the interface is almost identical, the Ras–RBD complex can be modeled with confidence by superimposing the experimental Ras structure on the Raps moiety in the Raps–RBD crystal complex. The interface structure in the resulting complex is stable over nanosecond molecular dynamics simulations in solution (Zeng et al., 1999) (see also below), and is essentially identical to that seen in the experimental Rap–RBD and Raps–RBD complexes. The Ras–RBD interactions seen in the simulations are also consistent with experimental chemical shift data (Emerson et al., 1995) for the Ras–RBD complex in solution (Fig. 3C), and with a large body of mutagenesis data (Zeng et al., 1999). The resulting Ras–RBD

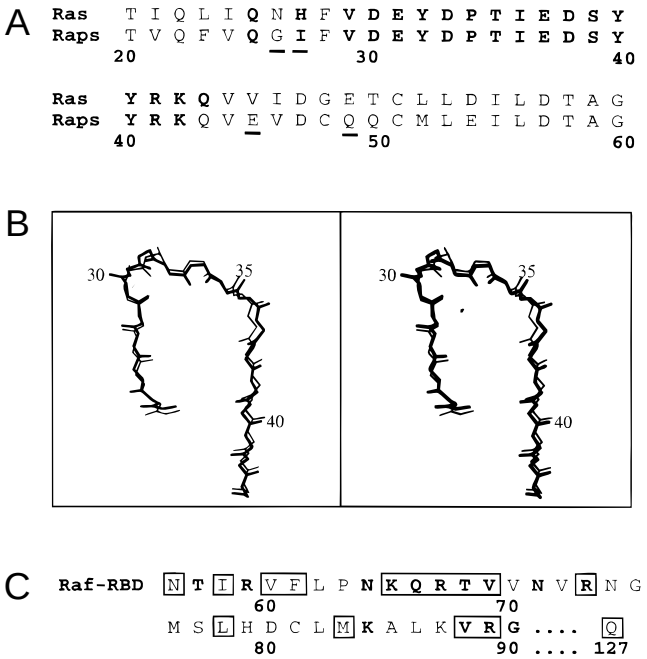


**Fig. 3. A:** Ras and Raps sequences in the interface region. Residues interacting directly with the RBD in the Raps–RBD complex are in bold. The four significant sequence differences in the region shown are underlined. In the Raps–RBD complex, residues 45 and 49 are fully solvated, and 12–14 Å away from the nearest RBD atom. Gly26 points away from the RBD, which is 8 Å away. **B:** Superposition of the backbone of residues 25–43 of Ras from the Ras crystal structure (thick line) and of Rap from the Raps–RBD crystal structure (thin line). The residues shown include all but one of the residues interacting directly with the RBD in the Raps-RBD complex. The RMS atomic deviation between the structures shown is 0.4 Å. **C:** Raf-RBD residues interacting with Ras in the simulations (bold) and in solution NMR experiments (boxed; from two-dimensional $^{1}$H–$^{15}$N HSQC experiments (Emerson et al., 1995)).

**Table 1.** *Radioactivity from Ras-GTP-$\gamma$-S:RBD-GST*

| Sample | Number of replicates[a] | Mean counts per minute (SD) | Ratio to native (%) |
|---|---|---|---|
| GST alone | 8 | 1,267 (176)[b] | 1.1 |
| Leu89 | 8 | 899 (173) | 0.7 |
| Wild-type | 8 | 120,280 (4,992) | 100 |
| Lys89 | 8 | 685 (110) | 0.6 |

[a]Quadruplicate samples were tested and the entire experiment was performed twice.

[b]Standard deviation; 1 $\mu$M Ras-GTP-$\gamma$-S and 0.69 $\mu$m GST-RBD constructs were used in the assay.

structure therefore provides a satisfactory basis for free energy simulations.

*Structure and dynamics of the native and mutant RBD*

In a previous paper, we investigated the structure and dynamics of the native and R89K mutant RBD (Zeng et al., 1998). Two stable conformations were found in the "Ras recognition helix" (RRH; residues 78–89), in agreement with the ensemble of NMR structures (Emerson et al., 1995). The earlier calculations were done with both the CHARMM19 and the OPLS/AMBER force fields. In the present work, we simulated the native RBD with the CHARMM22 force field, which models aliphatic hydrogens explicitly, unlike CHARMM19 and OPLS/AMBER. This improves the model, but doubles the cost of the simulations. In agreement with the earlier simulations, the RRH sampled two stable conformations during the 200 ps simulation: a fully helical conformation (with the helix extending to Arg89) and a turn conformation for residues 87–90. The helical conformation was stable for the first 120 ps, after which the 85–89 end of the RRH unwound. The helical backbone hydrogen bonds O84–H88 and O85–H89 broke simultaneously, with distances increasing to 4.6 and 4.1 Å, respectively, in good agreement with the previous simulations. In the H conformation, the Arg89 side chain packs against the RRH and hydrogen bonds to Thr68 and four water molecules. In the T conformation, three water molecules are inserted into the RRH between Ala85 and Arg89; the polar groups in the helix groove are more exposed to solvent, and the side chain of Arg89 is shifted into solvent, forming its maximum of five hydrogen bonds to water molecules.

For the R89K mutant, simulations with the CHARMM19 and OPLS/AMBER force fields were reported earlier (Zeng et al., 1998). In the H conformation, the Lys89 side chain packs alongside the RRH, close to the Arg89 position in the native H conformation. In the T conformation, Lys89 is much further out into solvent. Other parts of the protein are not significantly affected by the mutation, with a mean backbone RMSD between the native and mutant structures of about 0.7 Å (excluding the 90–95 flexible loop) in both the H and T conformations.

*Structure and dynamics of the Ras–RBD complexes*

Molecular dynamics simulations of the native Ras–RBD complex were carried out for 200 ps (following equilibration of the solvent) using both the CHARMM19 and CHARMM22 force fields. The native structure is very stable in both simulations. Structural information is summarized in Table 2. The average deviations from the initial structure, for protein backbone atoms outside the restrained buffer region, are 0.6 Å for the CHARMM22 run and 0.8 Å for the CHARMM19 run. The interface structure has RMSD of only 0.6–0.7 Å for backbone atoms and 1.2 Å for side chains. The Ras–RBD interactions are consistent (Fig. 3C) with the list of RBD residues whose H or N chemical shifts are perturbed upon Ras–RBD binding in solution (Emerson et al., 1995). A representative structure from the native CHARMM22 simulation is shown in Fig. 4A. The salt bridges that connect Ras and the RBD, Glu37–Arg67, Asp33–Lys84, and Asp38–Arg89, were preserved, as were the two backbone hydrogen bonds connecting the two antiparallel strands of the $\beta$-sheet that bridges the two proteins. Eleven interprotein hydrogen bonds (four involving Arg89) are found in the Ras–RBD interface, giving 0.9 hydrogen bonds per 100 Å$^2$ of interface area, typical of protein–protein complexes (Jones & Thornton, 1995). The RMS fluctuation of the protein atoms around their mean position is 0.40 Å for all heavy atoms and 0.38 Å for Arg89. For comparison to crystallographic *B*-factors, protein overall rotation and translation must be added in. Experimental estimates for lysozyme, pancreatic trypsin inhibitor, and ribonuclease A (Sternberg et al., 1979; Diamond, 1990; Howlin et al., 1990) give a 0.3–0.7 Å contribution to the RMS atomic fluctuations. Taken with the internal motion from the simulation, this gives a range of 13–21 for the average *B*-factor, which encompasses the average experimental value of 15.0 Å$^2$ (10.0 Å$^2$ for Arg89).

The side chain of residue 89 (RBD) remains in the same position throughout the simulations. Its interactions are in very good agreement with the Raps–RBD crystal structure (Nassar et al., 1995). The guanidinium group makes its maximum of five hydrogen bonds, forming a tight network bridging Ras and the RBD, which is essentially identical to that observed in the crystal structure (see Table 3). The Arg89 amino groups make one hydrogen

**Table 2.** *Structural statistics for the Ras–RBD complexes*

| | Ras–RBD | | Ras–R89K | | |
|---|---|---|---|---|---|
| | CHARMM19 | CHARMM22 | CHARMM19 | CHARMM22 | Experiment[a] |
| RMSD,[b] heavy atoms | 1.47 | 0.87 | 1.55 | 0.96 | |
| RMSD, backbone | 0.81 | 0.58 | 0.99 | 0.61 | |
| RMSD, side chain | 1.95 | 1.25 | 2.03 | 1.41 | |
| RMSD, interface backbone | 0.66 | 0.61 | 0.85 | 0.65 | |
| RMSD, interface side chain | 1.22 | 1.25 | 1.95 | 1.35 | |
| RMSF,[c] heavy atoms | 0.49 | 0.40 | 0.55 | 0.40 | |
| RMSF, residue 89 | 0.41 | 0.38 | 0.58 | 0.56 | |
| *B*-factor,[d] heavy atoms | 6.3 | 4.2 | 7.9 | 4.3 | 15.0 |
| *B*-factor, residue 89 | 4.5 | 3.8 | 8.8 | 8.2 | 10.0 |

[a]Experimental *B*-factor in Rap–RBD X-ray structure (Nassar et al., 1995). The discrepancy between calculated and observed *B*-factors is largely due to the lack of overall protein rotation and translation in the simulation (see text).
[b]RMS deviation (Å) from starting structure after 200 ps simulation.
[c]RMS fluctuation (Å) around mean structure during the last 100 ps of simulation.
[d]Å$^2$; calculated from the atomic fluctuations averaged over 100 ps of molecular dynamics.

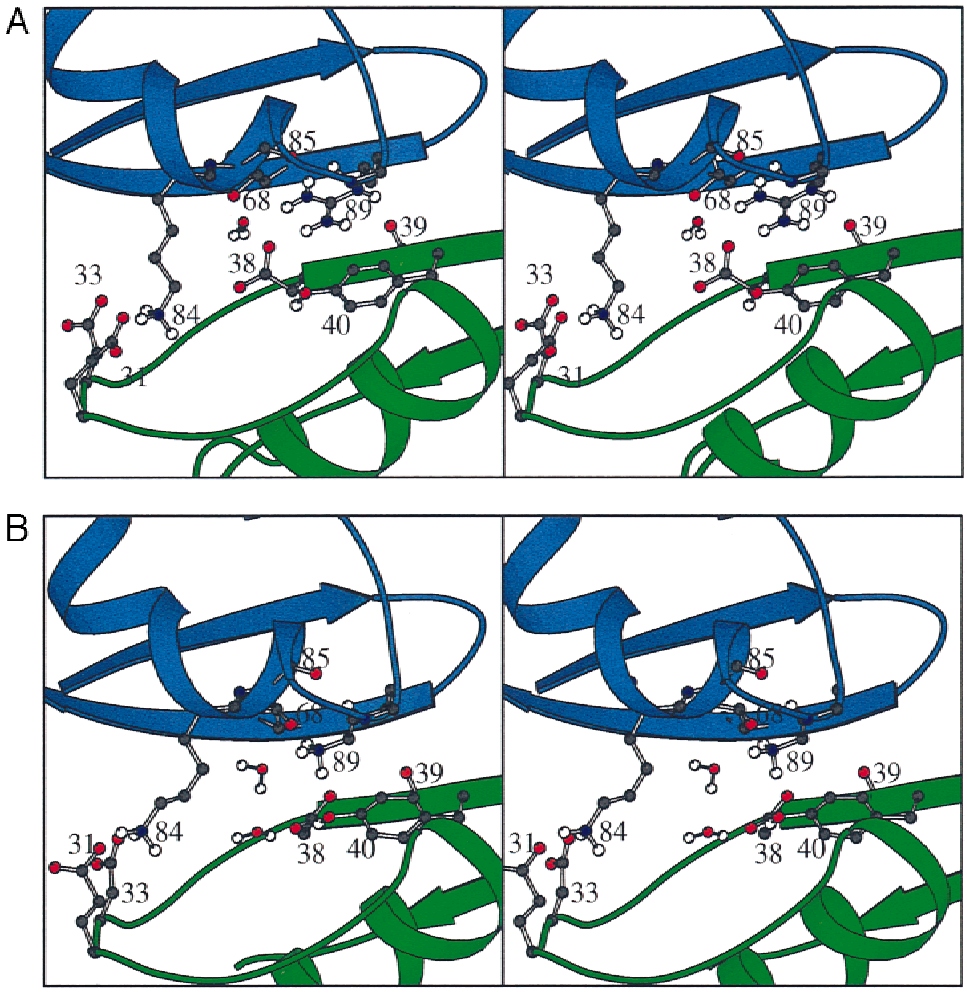


**Fig. 4. A:** Snapshot of the interface structure around Arg89 in the Ras–RBD complex, taken from the 200 ps CHARMM22 simulation of the native complex. Selected waters and side chains are shown. **B:** *Idem*, Ras–R89K complex.

bond to Asp38-OD1 and one to a stable water molecule that hydrogen bonds back to Asp38-OD2, also found in the crystal structure. One Arg89 amino group, as well as the NE group, hydrogen bond to Ser39-CO of Ras. Thus, four hydrogen bonds are made to Ras. A fifth is made to the Ala85-CO in the RBD, replacing the Ala85–Arg89 $\alpha$-helical hydrogen bond and linking the Arg side chain to the RRH. The Arg89 backbone amide continues to interact weakly with Ala85-CO, 3 Å away, and occasionally with Leu86-CO. The network of Arg89 interactions is further stabilized by stacking of the guanidinium group upon the aromatic ring of Ras/Tyr40. The aliphatic part of the side chain interacts with the side chains of RBD/Ala85, Val88, and Val62. Interestingly, while the Ras/Ser39-CO hydrogen bonds to Arg89, the $\beta$-sheet hydrogen bond that it would normally make to RBD/Arg67 on the neighboring $\beta$ strand is made by Ser39-OG instead.

A representative structure from the simulation of the mutant complex Ras–RBD(R89K) is shown in Figure 4B. Structural data are summarized in Table 2. At the end of the simulation, the mean RMSD of the (unrestrained) backbone atoms from the starting structure is 0.6 Å with the CHARMM22 force field and 1.0 Å with

**Table 3.** *Selected interatom distances in the Ras–RBD interface*

| Pair of atoms | | X-ray[a] | Simulation[b] |
|---|---|---|---|
| 89Arg-NH1[c] | Ser39-O | 2.89 | 2.90(16)[d] |
| 89Arg-NH2 | Ser39-O | 3.08 | 2.89(17) |
| 89Arg-NH2 | Asp38-OD | 2.66 | 2.69(01) |
| 89Arg-NH1 | WAT[e] | 2.85 | 2.86(12) |
| Asp38-OD | WAT[e] | 2.55 | 2.72(13) |
| Asp38-OD | 68Thr-OG | 2.60 | 2.66(13) |
| Glu37-O | 69Val-NH | 2.95 | 3.02(16) |
| Ser39-NH | 67Arg-O | 2.96 | 2.97(12) |
| Glu31-OE | 84Lys-NZ | 2.71 | 2.76(13) |
| Asp33-OD | 84Lys-NZ | 3.04 | 2.70(11) |

[a] Distance (Å) observed in Rap–RBD X-ray structure.
[b] Distance (Å) averaged over last 100 ps of the 200 ps molecular dynamics simulation of the native Ras–RBD complex.
[c] RBD residues have the residue number before the residue name. Other residues are from Ras.
[d] Standard deviation in significant digits.
[e] Water shown in Fig. 4A.

CHARMM19. Deviations for residues in the interface between the effector domain of Ras and the RRH region of the RBD are slightly greater than for the native complex, e.g., 0.7 Å for backbone atoms in the CHARMM22 simulation. The buried surfaces of the native and mutant complexes are 1,166 and 1,182 Å$^2$, respectively, typical of protein hetero-complexes (Jones & Thornton, 1995).

Compared to the native complex (Fig. 4A), the main structural changes are in the region around residue 89, as expected. The Lys89 side chain itself is 93% buried. Its ammonium is in the position occupied previously by one of the Arg89 amino groups. One ammonium hydrogen atom forms a hydrogen bond to Thr68-OG in the RRH, or occasionally to a water molecule. The second hydrogen bonds to Asp38-OD1 of Ras and the third, to a stable water molecule. This water molecule hydrogen bonds part of the time to Asp38-OD2, part of the time only to bulk water, and part of the time to another water which itself hydrogen bonds to Asp38-OD2. Thus, the bridging water structure between Lys89 and Ras/Asp38 still exists, but is much weaker than in the native complex, and only one strong hydrogen bond connects Lys89 to Ras. To compensate the lost Arg89–Ala85-CO hydrogen bond, the Ras recognition helix tightens: the O85–H89 hydrogen bond reforms, with the O–H distance decreasing from 3.0 to 2.2 Å, and Gly90 is incorporated into the helix. The aliphatic portion of the Lys89 side chain interacts with the side chains of Ras/Tyr40, RBD/Ala85, and Val62, as in the native complex. The Ras/Ser39-CO does not make any hydrogen bonds, whereas its side chain OG hydrogen bonds to the opposing RBD $\beta$ strand, as in the native complex (Fig. 4B). This network of interactions is mostly stable throughout 200 ps of simulation with both the CHARMM19 and CHARMM22 force fields. A few interactions break and reform during the simulations. In the CHARMM19 simulation, after 70 ps, Lys89 moves 2 Å into an alternate conformation and stays there for 20 ps before moving back. In this conformation, the Lys89–Asp38 hydrogen bond is broken and replaced by one to the RBD/Ala85-CO. In the CHARMM22 simulation, after 10 ps, the Lys89 ammonium moves 3 Å away from Asp38 and forms a hydrogen bond to the Ser39-CO for 15 ps before moving back.

### *Free energy simulations of the RBD*

We describe alchemical and conformational free energy calculations in this section and the next, corresponding to different legs of the thermodynamic cycles I and II in Figure 1. The upper cycle I involves only the RBD and connects the H and T conformations of the RRH in the native and R89K mutant RBD. The lower cycle II involves the binding of the native and mutant RBD to Ras.

#### *Horizontal legs of cycle I*

A detailed study of the conformational change from turn to helix in the RRH of the RBD has been described elsewhere (Zeng et al., 1998). It included H $\rightarrow$ T free energy simulations for the native and mutant RBD with both the CHARMM19 and the OPLS/AMBER force fields. These simulations represent the two horizontal legs of Cycle I. An additional H $\rightarrow$ T run was performed for the native RBD with the CHARMM22 force field, giving a free energy difference of 0.4 kcal/mol, in very good agreement with the CHARMM19 results (Zeng et al., 1998). Averaging over all the runs, the H $\rightarrow$ T free energy change for the native RBD is estimated to be $\Delta G_{\mathrm{RBD}}(\mathrm{H} \rightarrow \mathrm{T}) = 0.0 \pm 0.7$ kcal/mol.

Due to the agreement between the CHARMM19 and CHARMM22 results, the H $\rightarrow$ T leg for the mutant RBD was not repeated with CHARMM22. The earlier calculations gave $\Delta G_{\mathrm{R89K}}(\mathrm{H} \rightarrow \mathrm{T}) = -0.9 \pm 1.0$ kcal/mol. The difference between the OPLS/AMBER and CHARMM results for the upper leg (Zeng et al., 1998) almost cancels when the lower leg is subtracted. Averaging over all runs gives $\Delta\Delta G_{\mathrm{RBD}} = \Delta G_{\mathrm{R89K}}(\mathrm{H} \rightarrow \mathrm{T}) - \Delta G_{\mathrm{RBD}}(\mathrm{H} \rightarrow \mathrm{T}) = -0.75 \pm 0.65$ kcal/mol.

#### *Vertical legs of Cycle I*

The alchemical free energy calculations, where Arg89 is mutated into Lys89 or the reverse, correspond to the vertical legs of cycle I. Five runs were performed in the H conformation and four in the T conformation. The results are summarized in Table 4. The free energy derivatives $\langle \partial U/\partial \lambda \rangle_\lambda$ and the cumulative free energies $\Delta G(\mathrm{R} \rightarrow \mathrm{K})$ are shown as a function of $\lambda$ for each run in Figure 5. The agreement between runs and force fields is reasonable. The average $\Delta G_{\mathrm{H}}(\mathrm{R} \rightarrow \mathrm{K})$ is $-6.54 \pm 0.55$ and $-6.88 \pm 1.11$ kcal/mol in the H and T conformations, respectively. The side-chain dihedral angles sampled in the first windows of the mutation typically agreed with those obtained from conformational runs in the H and T states. In the last windows, the dihedral angles sampled agree with the earlier conformational runs on the R89K mutant. Thus, structures sampled at any given corner of the cycle are reasonably independent of the pathway taken to reach that endpoint.

The alchemical calculations provide another route to $\Delta\Delta G_{\mathrm{RBD}}$. The double free energy difference for the alchemical mutation in the two different conformations is $\Delta\Delta G_{\mathrm{RBD}} = \Delta G_{\mathrm{T}}(\mathrm{R} \rightarrow \mathrm{K}) - \Delta G_{\mathrm{H}}(\mathrm{R} \rightarrow \mathrm{K}) = -0.34 \pm 1.24$ kcal/mol, in good agreement with the value of $-0.75 \pm 0.65$ kcal/mol obtained from the conformational (horizontal) legs of cycle I. The closure error for the cycle is only 0.41 kcal/mol. Overall, the mutation is predicted to stabilize by 0.5–0.6 kcal/mol the H conformation thought to be required for binding (Nassar et al., 1995). The uncertainty of the calculation, from the dispersion between runs, is somewhat larger than the predicted stabilization.

For the R $\rightarrow$ K free energy difference, averaging over the H and T conformations with the appropriate Boltzmann weighting (see Materials and methods), we obtain $\Delta G_{\mathrm{RBD}}(\mathrm{R} \rightarrow \mathrm{K}) = -6.74$ kcal/mol ($-6.46$ kcal/mol from the CHARMM19 runs and $-7.21$ kcal/mol from the CHARMM22 runs).

#### *Structures sampled and free energy components*

To characterize the interactions of the 89 side chain with its surroundings, Figure 6 shows the interaction energy of this side chain with groups in radial shells around it. The largest interactions involve groups in the first solvation shell; these groups are all waters in both the Lys and Arg cases in the T conformation. In the H conformation, one Arg first shell water is replaced by protein (Thr68). The interaction energy with the first shell is $-72$ kcal/mol for Lys and $-94$ for Arg in the T conformation. However, more distant groups also make large contributions. The second shell contributes $-54$ kcal/mol for Lys and $-5$ for Arg. Integrating the interaction energy over increasingly distant shells, the Lys89 interaction energy does not become systematically more favorable than the Arg89 energy until beyond 7 Å (Fig. 6B).

To relate these interactions to the free energy change, group contributions to the total free energy change are calculated (see Materials and methods). The free energy changes are dominated by solvent contributions (Table 5). In the T conformation, the side chain of Arg89 is fully solvated, with five hydrogen bonds to water molecules. When Arg89 is mutated to Lys, two hydrogen bonds are lost. At the same time, the delocalized Arg positive charge is

**Table 4.** *Alchemical free energy changes in the free Ras binding domain*[a]

| Run | Run direction[b] | RRH conformation[c] | Force field | $\Delta G_{RBD}(R \rightarrow K)$ |
|---|---|---|---|---|
| 1 | R → K | H | CHARMM19 | −6.70 |
| 2 | K → R | H | CHARMM19 | −5.79 |
| 3 | R → K | H | CHARMM19 | −7.06 |
| 4 | K → R | H | CHARMM19 | −6.02 |
| 5 | R → K | H | CHARMM22 | −7.14 |
| | Average over runs 1–4 | H | CHARMM19 | −6.39 (0.50) |
| | Average over runs 1–5 | H | | −6.54 (0.55) |
| 6 | R → K | T | CHARMM19 | −6.12 |
| 7 | K → R | T | CHARMM19 | −6.90 |
| 8 | R → K | T | CHARMM22 | −5.81 |
| 9 | K → R | T | CHARMM22 | −8.66 |
| | Average over runs 6–7 | T | CHARMM19 | −6.51 (0.39) |
| | Average over runs 8–9 | T | CHARMM22 | −7.24 (1.43) |
| | Average over runs 6–9 | T | | −6.88 (1.11) |
| Boltzmann average,[d] runs 1–4, 6–7 | | | CHARMM19 | −6.46 |
| Boltzmann average, runs 5, 8–9 | | | CHARMM22 | −7.21 |
| Boltzmann average, all runs | | | | −6.74 |

[a] Free energies in kcal/mol.
[b] Direction of free energy simulation.
[c] Conformation of the Ras recognition helix in Raf.
[d] Boltzmann average over H and T results, from Equation 4.

replaced by the Lys charge concentrated on the smaller ammonium group. This changes the free energy by ca. −8.1 ± 1.3 kcal/mol, −5.5 kcal/mol of which arise from electrostatic interactions. A recent computational study of amino acids in solution specifically compared the stabilization of the Arg and Lys charges in water, giving a −6.9 kcal/mol free energy difference in favor of the more localized Lys charge (Nina et al., 1997), close to the value obtained here. In the H conformation, where Arg89 forms only four hydrogen bonds to solvent, the solvent free energy contribution is increased to −7.2 kcal/mol.

### *Free energy simulations of the complex*

#### *Free energy changes*

Alchemical free energy runs in the Ras–RBD complex correspond to the rightmost vertical leg in Cycle II (Fig. 1). Results from six runs are summarized in Table 6. The free energy derivatives and free energy curves are shown in Figure 5. The free energy results from different runs vary between −2.3 and −5.7 kcal/mol. The average $\Delta G_{Com}(R \rightarrow K)$ is −3.87 ± 1.21 kcal/mol (−4.68 ± 0.99 kcal/mol for two CHARMM19 runs and −3.47 ± 1.11 for four CHARMM22 runs). Subtracting the free energy result for the RBD in solution, we find that the binding free energy of the Ras–RBD complex increases by 2.9 kcal/mol due to the Arg89 → Lys mutation (1.8 kcal/mol with CHARMM19; 3.7 kcal/mol with CHARMM22). The experimental value is 3.0 kcal/mol or more, in good agreement with the CHARMM22 calculations, and rough agreement with the CHARMM19 ones.

The induced ordering of the RBD upon binding contributes only slightly (0.2 kcal/mol) to the overall result, because the $\Delta\Delta G_{RBD}$ for cycle I is only 0.5–0.6 kcal/mol. While this contribution is smaller than the computational uncertainty, its exact magnitude could not be anticipated before doing the calculations.

#### *Structures sampled and free energy components*

The structures sampled in the free energy simulations are in good agreement with the simulations discussed above (Fig. 4A,B). The position of the Arg89 side-chain position was maintained over the seven windows (of total duration 340 ps) of all six free energy runs. As the Lys89 side chain was "grow in" in the three forward runs, it adjusted its position toward structures close to that seen in the earlier simulation of the Ras–R89K complex (Fig. 4B), with some variations however. The structures sampled in runs 1–4 (Table 6) are similar to that shown in Figure 4B, but the Lys89 hydrogen bond to water is replaced by one to Ala85-CO, similar to Arg89 in the native complex. In run 3, the carboxylate of Asp38 hydrogen bonds to RBD/Thr68 and to Tyr40 of Ras. In runs 5–6, the Lys endpoint simulation sampled a somewhat different structure, in which the Lys89 ammonium hydrogen bonds to both Ser39-CO and Asp38-OD1, like Arg89 in the native complex. Thus multiple conformations are available for Lys89, in contrast to Arg89. The hydrogen bond partners of Lys89 at the Lys endpoints of the different runs are listed in Table 7 along with the number of nearby waters. The solvent environment of Lys89 varies significantly between runs, depending on the force field used. The CHARMM19 force field (which treats aliphatic hydrogens implicitly) leads to two waters within 3.5 Å of the Lys89-NZ and another within 5.5 Å. With the CHARMM22 force field (which treats aliphatic hydrogens explicitly), there is only one water within 5 Å and another within 5.5 Å. Two typical structures are shown in Figure 7. The differences appear to be due to steric repulsion in the CHARMM22 runs between water and aliphatic groups around Lys89, such as RBD/Val62. They lead to very different solvent contributions to the free energy change (Table 5). A correlated change occurs for Tyr40, which hydrogen bonds to Lys89 only in the CHARMM22 runs, where it replaces one of the nearby waters seen in the CHARMM19 runs (Fig. 7). Given the improved treatment of sol-

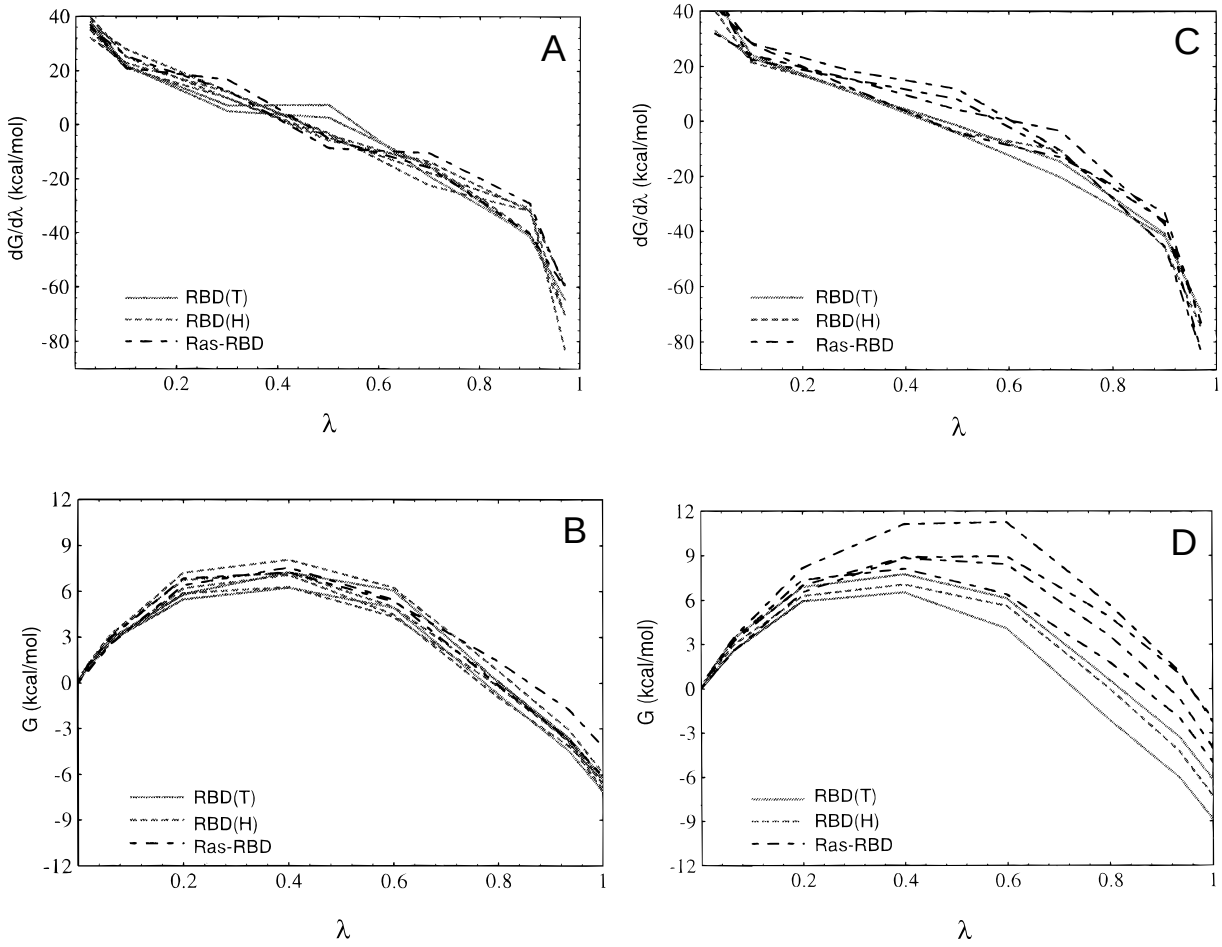


**Fig. 5. A:** Alchemical free energy derivatives during the Arg89 → Lys mutation from the CHARMM19 simulations. **B:** Cumulative free energy change $\Delta G(\mathrm{R} \rightarrow \mathrm{K})$ as a function of $\lambda$ from the CHARMM19 simulations. **C:** Alchemical free energy derivatives during the Arg89 → Lys mutation from the CHARMM22 simulations. **D:** Cumulative free energy change $\Delta G(\mathrm{R} \rightarrow \mathrm{K})$ as a function of $\lambda$ from the CHARMM22 simulations.

vation provided by the CHARMM22 force field for other systems (Mackerell et al., 1995, 1998), the structures observed with this force field are thought to be the more realistic.

The radial distribution of groups interacting with residue 89 is very different in the complex from that in the free RBD. The interaction energies of groups in radial shells around the 89 side chain are plotted in Fig. 6 for both the Arg and Lys moieties, in the complex and the free RBD. The Arg interaction energies are taken from the Arg endpoint of free energy run 3 (where it has a weight of 0.97), while the Lys interaction energies are taken from the Lys endpoint of run 3. In the free RBD (T conformation), the water oxygen and hydrogen atoms produce large peaks of opposite signs between 2.5 and 4 Å from the Lys89-NZ, or 3–5 Å from the Arg89-CZ, corresponding to the first solvation shell of each moiety. The second shell extends out to 5.5 Å for Lys and 6 Å for Arg, and gives smaller, broader peaks. For Arg89, the interaction energies with groups out to 6 Å are approximately equivalent in the complex and in the free RBD. In contrast, the Lys89 interactions are very different in the two environments, with stronger first shell interactions in the complex, but weaker second shell interactions.

The structural differences between runs lead to differences in the free energy components. Variations of the RBD contribution arise from charged residues near the electrostatic cutoff sphere of residue 89, as an artifact of the electrostatic cutoff. For example, residue 89 is within the cutoff sphere of Glu30 during the first part of run 3; during the last two windows, the Arg89 moiety drifts out of the Glu30 cutoff sphere, which continues to interact with Lys89, however. Such contributions (e.g., from Ras/Glu30, RBD/Asp80, RBD/Glu94) largely cancel with other residues near the cutoff sphere, and none of them leads to any significant systematic error in the free energy. The variation of solvent contributions can be almost entirely accounted for by the 2–3 water molecules with specific interactions with residue 89, which vary between runs in a force field-dependent way, as discussed (see Table 7). Variations for other residues arise either as a result of the different solvent and hydrogen bonding structures around residue 89 (e.g., Ras/Tyr40 hydrogen bonds to Lys89 moiety in the CHARMM22 but not the CHARMM19 runs), or as a result of noisy van der Waals endpoint contributions (e.g., Ras/Asp30).

Five residues consistently give large, almost entirely electrostatic contributions to the free energy change: Glu37, Ser39, and Arg41 of Ras, and Lys84 and Lys87 of Raf. All but Ser39 are rather distant from the mutation site. Ser39 interacts with Arg89 through a bifurcated hydrogen bond to its backbone CO (Fig. 4A), and

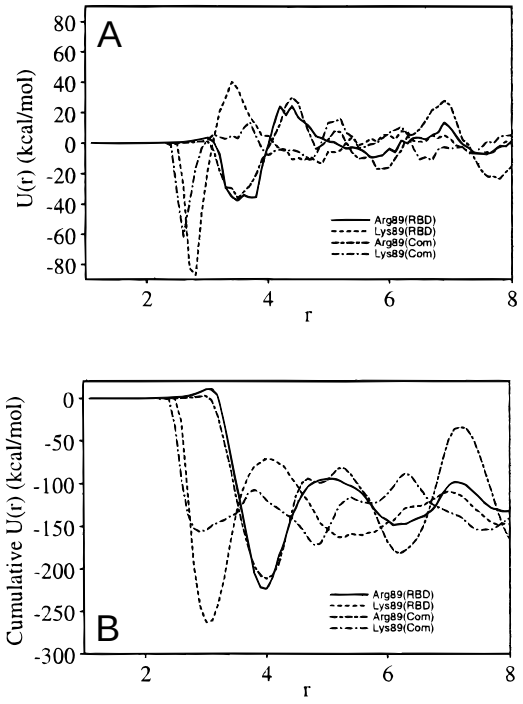


**Fig. 6.** Radial distribution of interaction energies between residue 89 and its environment. The distance $r$ (Å) is calculated from the Arg89-CZ or the Lys89-NZ, as appropriate. **A:** Interaction energy with groups in the radial shell within $r - 0.25$ Å and $r + 0.25$ Å of 89. **B:** Interaction energy integrated radially from 0 to $r$.

makes the largest single residue contribution to the free energy (with the exception of the large Asp38 van der Waals contribution in some runs): 3.9 kcal/mol favoring Arg89, including a 5 kcal/mol electrostatic contribution. Arg41 favors Lys, while Glu37, Raf/Lys84 and Lys87 favor Arg by about 2 kcal/mol, due to Coulombic interactions over distances of 8–9 Å.

## Discussion

### *Uncertainty in the free energy calculations*

Uncertainty in free energy calculations stems from many sources and is notoriously hard to estimate (van Gunsteren & Weiner, 1989); at the same time its magnitude is very important to judge the predictive power of free energy simulations. The numerous runs performed here with different force fields allow a reasonable uncertainty estimate to be made.

For a mutation that conserves the net electrostatic charge, as here, the computed free energies are not expected to be very sensitive to the exact treatment of electrostatic interactions, as long as it is reasonable. We showed earlier that increasing the electrostatic cutoff distance from 13 to 16 Å had little effect on the calculated conformational free energies of the RBD (Zeng et al., 1998). In addition, a nanosecond simulation of the native Ras–RBD complex was performed with no truncation of electrostatic interactions, which sampled conformations in good agreement with the ones reported here (Zeng et al., 1999).

Force field dependency is seldom examined explicitly in free energy simulations, due to cost. It was explored in detail here and in (Zeng et al., 1998) by performing free energy calculations with three commonly-used force fields: CHARMM19 (Brooks et al., 1983), OPLS/AMBER (Jorgensen & Tirado-Rives, 1988; Weiner et al., 1984), and CHARMM22 (Mackerell et al., 1998). The first two treat aliphatic hydrogens implicitly, the last is an "all-hydrogen" force field that considers aliphatic hydrogens explicitly. The CHARMM22 force field gave better agreement with experiment than CHARMM19 for the overall binding free energy change. Some differences were observed in the structures sampled with the different force fields; for example, CHARMM22 leads to a broader free energy well for the H conformation of the RRH than CHARMM19 and OPLS/AMBER (Zeng et al., 1998). However, CHARMM19 and CHARMM22 give reasonable agreement for the chemical and conformational free energies. OPLS/AMBER gave H $\rightarrow$ T free energies for the RBD that differed by ca. 1.5 kcal/mol from CHARMM19 and CHARMM22. However, the differences cancelled almost exactly when the results for the native and mutant RBD were subtracted (Zeng et al., 1998). Thus, the experimentally relevant double free energy difference $\Delta\Delta G = \Delta G_{Com}(\mathrm{R} \rightarrow \mathrm{K}) - \Delta G_{\mathrm{RBD}}(\mathrm{R} \rightarrow \mathrm{K})$ is likely to be less sensitive to force field details than its individual components. This is confirmed by comparing the CHARMM19 and CHARMM22 $\Delta\Delta G$'s (Tables 4, 6). Thus, we expect that deviations in $\Delta\Delta G$ due to a change of force field will be at most of the same order as the 1.5 kcal/mol deviation observed above for the individual H $\rightarrow$ T free energies.

To ensure good conformational sampling, several approaches were used. First, we systematically identified and studied individually the most stable conformations of the Arg89 region of the free RBD (Zeng et al., 1998). The existence of two stable conformations, suggested by the ensemble of NMR structures (Emerson et al., 1995), was confirmed, and their effect on Ras–RBD binding was explicitly included in the present calculations of $\Delta\Delta G$ through the thermodynamic Cycle I (Fig. 1). Second, we performed long molecular dynamics simulations (reported elsewhere (Zeng et al., 1999)) in which all the RBD and most of Ras were explicitly included and solvated. These calculations suggest that no significantly different stable conformation of the Arg89 region exists in the complex that might contribute to the binding affinity. Third, we performed a large number of free energy runs under different conditions and along several different pathways. For example, the four legs of cycle I were simulated a total of 18 times, representing over 7.5 ns of molecular dynamics simulation. The horizontal and vertical legs represent very different pathways through chemical and conformational space, yet they gave very similar results (within 0.4 kcal/mol) for the double free energy difference $\Delta G_{\mathrm{T}}(\mathrm{R} \rightarrow \mathrm{K}) - \Delta G_{\mathrm{H}}(\mathrm{R} \rightarrow \mathrm{K})$. Structures at the endpoints of the different runs were consistent, and no large structural "hysteresis" was observed.

Other sources of uncertainty were monitored as well. Extrapolation of the free energy derivatives to the endpoints ($\lambda = 0.97 \rightarrow 1$ and $0.03 \rightarrow 0$), where they vary rapidly, was performed both using the theoretical shape predicted for van der Waals liquids (Simonson, 1993; Resat & Mezei, 1994) and a linear response approximation; the free energy results differed typically by 0.5–1.0 kcal/mol. Free energy hysteresis effects were moderate, as seen by comparing forward and backward runs in Tables 4 and 6. Some systematic cancellation of this error is known to occur when runs in opposite directions are averaged. The overall uncertainty arising from limited sampling, numerical integration, time-lag hysteresis, and other effects not related to the choice of force field is probably reflected accurately by the deviation between the individual free

**Table 5.** *Group contributions to the free energy changes*[a]

| | Free RBD, helical conformation[b] | | | Free RBD, turn conformation[b] | | |
|---|---|---|---|---|---|---|
| Group | vdW[c] | Elec[d] | Total[e] | vdW[c] | Elec[d] | Total[e] |
| Water | −1.78(0.02) | −5.39(1.49) | −7.17(1.47) | −2.68(0.63) | −5.46(1.53) | −8.14(1.3) |
| RBD | 1.15(0.71) | −0.53(1.13) | 0.62(1.80) | 0.85(0.30) | 0.20(0.85) | 1.05(1.0) |
| Residue 89[f] | −0.1 | 0.3 | 0.2 | | | |
| | Ras–RBD complex[g] | | | | | |
| | CHARMM19 | | | CHARMM22 | | |
| Group | vdW | Elec | Total | vdW | Elec | Total |
| Water | 0.26(0.03) | −12.22(0.30) | −12.0(1.29) | −1.03(0.76) | 1.09(2.80) | 0.07(2.10) |
| RBD | 1.88(1.00) | −1.74(1.65) | 0.14(0.67) | 0.28(1.38) | 6.70(4.22) | 6.99(3.22) |
| Ras | 0.82(0.15) | 5.87(1.44) | 6.69(1.59) | −5.29(0.96) | −5.65(4.42) | −10.50(4.80) |
| Residue 89[f] | 0.3(0.2) | 0.2(0.0) | 0.5(0.2) | 0.1(0.2) | −1.0(0.2) | −1.1(0.4) |
| **Glu37** | 0.1(0.0) | 2.3(0.4) | 2.4(0.5) | 0.0(0.0) | 1.4(0.8) | 1.5(0.8) |
| **Asp38** | −1.7(0.6) | 0.3(0.2) | −1.4(0.8) | −4.7(0.5) | −1.0(1.8) | −5.7(1.4) |
| **Ser39** | −0.2(0.0) | 4.4(0.4) | 4.2(0.3) | −2.2(0.2) | 5.7(2.5) | 3.5(2.5) |
| **Tyr40** | 2.1(0.3) | −0.5(0.0) | 1.6(0.3) | 1.9(0.4) | −3.7(0.2) | −1.8(0.3) |
| Tyr40(ring) | 1.4(0.4) | 0.0(0.0) | 1.4(0.4) | 1.2(0.5) | −1.2(0.8) | 0.1(1.2) |
| **Arg41** | 0.1(0.0) | −3.2(0.2) | −3.1(0.2) | 0.1(0.0) | −1.7(0.6) | −1.7(0.5) |
| Asp57 | 0.0(0.0) | 0.0(0.1) | 0.1(0.1) | 0.1(0.0) | −1.4(0.6) | −1.4(0.6) |
| 67Arg[h] | 0.5(0.1) | −0.1(0.1) | 0.4(0.2 | −0.6(0.4) | −0.8(1.2) | −1.3(0.7) |
| **84Lys** | 0.1(0.0) | 1.6(0.2) | 1.7(0.2) | 0.1(0.1) | 2.4(1.3) | 2.5(1.4) |
| 85Ala | −0.3(0.4) | −0.4(0.2) | −0.6(0.5) | −0.4(0.2) | 1.9(1.5) | 1.4(1.2) |
| **87Lys** | 0.0(0.0) | 1.6(0.1) | 1.7(0.1) | 0.0(0.0) | 1.3(0.7) | 1.3(0.7) |
| Glu30[i] | 0.0(0.0) | −0.8(0.2) | −0.8(0.2) | 0.0(0.0) | −5.5(1.2) | −5.5(1.2) |
| 94Glu | 0.0(0.0) | 2.0(0.4) | 2.0(0.4) | 0.0(0.0) | 6.0(4.5) | 6.0(4.5) |
| 80Asp | 0.0(0.0) | −4.5(1.2) | −4.5(1.2) | 0.0(0.0) | −0.4(0.2) | −0.4(0.2) |

[a]kcal/mol. The residues with the largest contributions are in bold. Residues with contributions less than ±1 kcal/mol are not included (other than 89).
[b]Contributions to $\Delta G(\mathrm{R} \rightarrow \mathrm{K})$ in the free RBD in solution with the RRH in the H or T conformation, averaged over all runs (CHARMM19 and CHARMM22).
[c]van der Waals contribution.
[d]Electrostatic contribution.
[e]Total contribution.
[f]Contribution of side-chain–backbone interactions within residue 89.
[g]Contributions to $\Delta G(\mathrm{R} \rightarrow \mathrm{K})$ in the Ras–RBD complex, averaged over either the CHARMM19 or CHARMM22 runs, as indicated. Standard errors in parentheses.
[h]RBD residues have the residue number before the residue name. The other residues are from Ras.
[i]Residues making large contributions near the cutoff sphere of residue 89 (see text) are grouped in the bottom part of the table.

energy runs performed with a given force field, namely 1–1.2 kcal/mol. Together with the 1.5 kcal/mol uncertainty associated with the choice of force field, this gives an overall estimated uncertainty of about 1.9 kcal/mol.

### *Free energy component analysis and structural contributions to the binding free energy change*

The simulations can be used to provide microscopic insights into binding that are not available experimentally, in particular through the analysis of group free energy contributions, or "components." Such free energy components are not state functions, as first pointed out by Simonson and Brünger (Simonson & Brünger, 1992; Hodel et al., 1993) and analyzed in detail by others (Boresch et al., 1994; Mark & Gunsteren, 1994; Brady et al., 1996; Archontis & Karplus, 1996), but depend on the pathway used to connect the initial and final states of the system. The free energy contributions of individual residues or structural groups also present a larger statistical uncertainty and force field dependency than the overall free energy change. All three aspects are illustrated by the large variations of the Asp38 and Tyr40 contributions discussed above (Table 5). For example, the large negative van der Waals contribution of Asp38 in the CHARMM22 runs is pathway dependent; it arises from steric overlap with the disappearing Arg89 moiety when $\lambda \geq 0.97$, and would be greatly reduced if a different mutation pathway were used, in which the Arg side chain were constrained to overlap with the Lys moiety. In addition, the free energy contribution of an individual group arises from terms in the energy function representing direct interactions with the mutated side chain, and so it should be thought of as a "direct" free energy contribution. Groups

**Table 6.** *Alchemical free energy changes in the Ras–RBD complex*[a]

| Run | Direction | Force field | $\Delta G_{Com}(R \rightarrow K)$ |
|---|---|---|---|
| 1 | R → K | CHARMM19 | −5.67 |
| 2 | K → R | CHARMM19 | −3.69 |
| 3 | R → K | CHARMM22 | −2.51 |
| 4 | K → R | CHARMM22 | −4.10 |
| 5 | R → K | CHARMM22 | −2.31 |
| 6 | K → R | CHARMM22 | −4.93 |
| Average over runs 1–2 | | CHARMM19 | −4.68 (0.99) |
| Average over runs 3–6 | | CHARMM22 | −3.47 (1.11) |
| Average over runs 1–6 | | | −3.87 (1.21) |
| | | Force field | $\Delta\Delta G(R \rightarrow K)$[b] |
| Average | | CHARMM19 | 1.78 (1.12) |
| Average | | CHARMM22 | 3.74 (1.81) |
| Average over all runs | | | 2.87 (1.33) |
| Experiment | | | ≥3.0 |

[a]Free energies in kcal/mol.

[b]$\Delta\Delta G(R \rightarrow K) = \Delta G_{Com}(R \rightarrow K) - \Delta G_{RBD}(R \rightarrow K)$ is the double free energy difference for the thermodynamic cycle II (Fig. 1).

that do not interact directly with residue 89 can still affect the free energy by interacting with other, directly interacting groups (Archontis et al., 1998). Because of this, the free energy components cannot be directly translated into "interaction free energies," contributing to binding in a simple way and transferable from one structure to another. Nevertheless, this study and others show that the free energy components are sufficiently robust to be qualitatively useful as long as a reasonable pathway is chosen, such as the simple alchemical pathway used here (Lau & Karplus, 1994; Boresch & Karplus, 1995; Sun et al., 1996; Archontis et al., 1998).

The binding free energy change due to the Arg89 → Lys mutation arises from a number of competing effects in the free RBD and in the complex (Table 5). In the free RBD, Arg89 and Lys89 are both exposed to solvent (fractional solvent accessible surfaces 60 and 70%), making 4–5 and 3 hydrogen bonds to water, respectively. Protein residues, including 89, make small contributions to the free energy change (<1 kcal/mol; not shown). The mutation cost of −6.7 kcal/mol is thus largely due to differences in solvation of the Arg and Lys side chains, with the solvent contribution representing 80–90% of the total free energy change (Table 5). The largest interactions with the 89 side chain are within its first solvation shell (Fig. 6). However, more distant interactions are also important for differentiating Arg and Lys. Thus, integrating radially the difference between the Arg and Lys interaction energies, Lys is favored systematically only beyond 7 Å.

In the native complex, four hydrogen bonds connect Arg89 to Ras, with a fifth between Arg89 and the RRH backbone (Table 3). An ordered water bridges Arg89 and Asp38, with a calculated *B*-factor of 13 Å$^2$, slightly lower than the observed 16 Å$^2$. This arrangement is maintained throughout all six free energy runs. Lys89 is also connected to Asp38 by 1–2 waters, but more weakly; Lys89 makes one other hydrogen bond to Ras and a third to bulk water. Thus, the mutation removes 2–3 hydrogen bonds between Ras and the RBD. One of these is balanced by an additional hydrogen bond in the mutant RRH. The increased mobility of Lys89 compared to Arg89 helps to stabilize the mutant complex entropically, although the exact extent of this effect cannot be estimated from the simulations. Comparing the interaction energies of Arg89 and Lys89 with their surroundings in the complex and the free RBD (Fig. 6), the short- and medium-range Arg89 interactions are similar, while Lys89 has more favorable first-shell interactions in the complex, but less-favorable second-shell interactions.

The residue free energy contributions in Table 5 reflect these structural features. Overall, most of the R → K free energy change in the complex comes from residues 37–41 in the conserved effector domain of Ras, Lys84, and Lys87, which are conserved in Raf, and a few water molecules interacting specifically with residue 89. The contributions of Ras/Tyr40, RBD/Ala85, and the specific waters vary strongly between runs in a correlated and force field-dependent way, compensating each other mutually to a large extent. Glu37, Arg41, RBD/Lys84, and RBD/Lys87 contribute through long-range electrostatic interactions over distances of 8–9 Å. Ras/Ser39 makes the largest single-residue contribution, 3.9 kcal/mol favoring Arg89, due to the strong bifurcated hydrogen bond of Arg89 to its backbone CO which is lost in the R89K mutant.

**Table 7.** *Local environment around Lys89 during free energy simulations*[a]

| Run number | 1,2[b] | 3,4 | 5,6 |
|---|---|---|---|
| Force field | CHARMM19 | CHARMM22 | CHARMM22 |
| Hydrogen | Asp38-OD1 | Asp38-OD1 | Asp38-OD1 |
| Bond | Ala85-O | Ala85-O | Ala85-O |
| Donors | Water | Tyr40-OH | Ser39-O |
| Waters < 3.5 Å[c] | 2.0 | 0.5 | 0.3 |
| Waters < 5.0 Å[c] | 2.2 | 1.2 | 1.2 |
| Waters < 5.5 Å[c] | 2.9 | 1.9 | 2.3 |
| $\Delta G$, waters < 5.5 Å[d] | −7.0 | −0.2 | |

[a]Results from the Lys89 endpoints of the free energy runs.

[b]Runs 1, 2 share the same Lys endpoint, since run 2 was initiated from the Lys endpoint of run 1; similarly for runs 3, 4 and 5, 6.

[c]Average number of water molecules within specified distance of Lys89-NZ.

[d]Contribution of waters within 5.5 Å of Lys89-NZ to the free energy change $\Delta G_{Com}(R \rightarrow K)$ (kcal/mol).

## Conclusions

The simulations of the R89K mutation in Raf are compatible with the experimental lower bound for the free energy change (particularly the CHARMM22 calculations), with an estimated computational uncertainty of <2 kcal/mol. The environment of the mutation site in the native simulations is in excellent agreement with the Rap–RBD and Rap(E30D,K31E)–RBD crystal structures. The simulations provide models of the native and mutant RBDs in complex with Ras, and suggest that they differ only slightly from the native Rap–RBD complex and from the Rap(E30D,K31E)–RBD mutant complex. This is a result of the high sequence conservation between Ras and Rap, especially in the interface region.

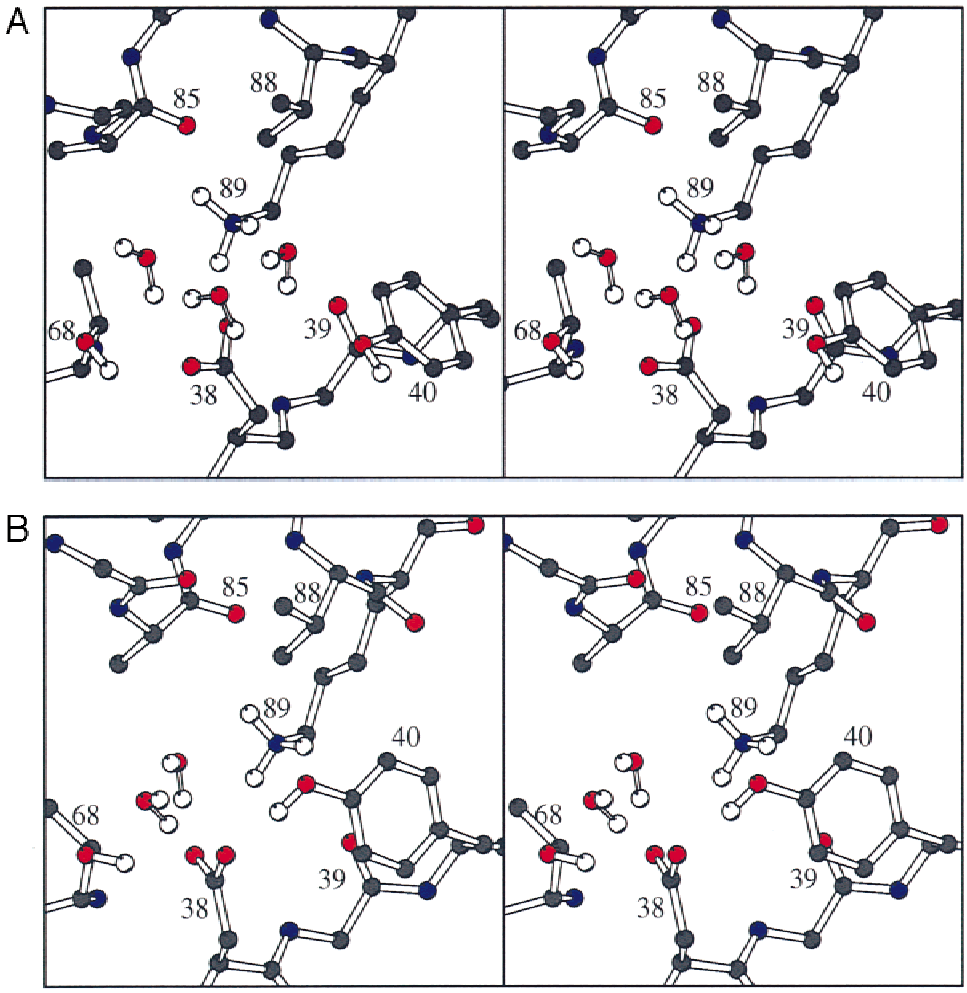


**Fig. 7.** Environment around Lys89 with two different force fields. **A:** Lys endpoint of the CHARMM19 run 1 (aliphatic hydrogens treated implicitly). **B:** Lys endpoint of the CHARMM22 run 3 (aliphatic hydrogens treated explicitly).

The alchemical simulations of the free RBD show that there is a considerably greater free energy cost (6–7 kcal/mol) to desolvate the localized charge of the Lys ammonium group than the larger Arg charge. This effect represents roughly 10% of the solvation free energy of the Lys analogue, methyl-ammonium. This effect is nonspecific and is expected to play a general role in protein–protein interfaces, which can help to explain the greater propensity of Arg to be found in such interfaces than Lys (Janin et al., 1988).

In the Ras–RBD complex, most of the Arg/Lys89 "solvation" is provided by protein side chains and 2–3 neighboring waters. The most prominent single-residue contribution is 3–4 kcal/mol from Ras/Ser39. However, groups as much as 8–9 Å away also make large contributions. Overall, the main contributions arise from the conserved residues 37–41 in the effector domain of Ras, the conserved Lys84 and Lys87 of Raf, and the 2–3 waters interacting specifically with 89. The many different contributions to the R $\rightarrow$ K binding free energy difference show that the effect of the mutation is not adequately described by a simple counting of hydrogen bonds. The free energy simulations can indeed reveal "hidden thermodynamics," as suggested by Gao et al. (1989).

## Materials and methods

### *Experimental*

#### *Mutagenesis of RBD-89*

RBD-89 mutants were constructed by PCR site-directed mutagenesis (Higuchi et al., 1988; Ho et al., 1989), using c-Raf-1 cDNA as a template. Oligonucleotides were synthesized incorporating the desired mutations, as well as EcoRI restriction sites at the 5′ end to facilitate subcloning into the pGEX-2TH vector (Maruta et al., 1991) linearized with EcoRI. Mutations were verified by nucleotide sequencing.

#### *Expression and purification of GST-RBD constructs and Ras*

V-Ha-Ras was purified from *Escherichia coli* according to the procedure of Gibbs et al. (1984). The concentration of Ras was determined with the Bio-Rad protein assay (Bio-Rad Laboratories, Hercules, California). To replace the residues 89 (Arg) of RBD by Leu or Lys, PCR-mediated mutagenesis was performed as described previously (Maruta et al., 1991). The wild-type RBD and

its mutants (Leu89 or Lys89) were produced in *E. coli* as a GST fusion, and were affinity-purified on GSH-beads (Fridman et al., 1994). The concentrations of GST-RBD constructs on beads were determined by scanning Coomassie-stained SDS-PAGE by densitometry (Molecular Dynamics 300 Series computing densitometer) and measuring band densities relative to BSA standards with ImageQuant 3.3 (Molecular Dynamics). The folding of the mutant proteins was not tested here, but the Leu89 mutant was shown previously by circular dichroism spectroscopy to adopt a native-like fold (Block et al., 1996), and the Lys89 mutant is presumed to be still more native-like.

*In vitro assay for binding Ras-GTP*

Binding between Ras and RBD-GST constructs was carried out as previously described (Fridman et al., 1994). Several modifications to the method were included in the present work. Briefly, v-Ha-Ras was labeled with GTP-$\gamma$-$S^{35}$ (Du Pont). A PD-10 column (Pharmacia, Biotech) was used to remove unbound GTP-$\gamma$-S from the labeling mix. Labeled Ras was then added to GST-RBD constructs bound to agarose beads. Extra glutathione-agarose beads were added to the binding mix: 50 $\mu$L of 50% slurry. The reaction mixtures were shaken at room temperature for 1 h. Free Ras-GTP-$\gamma$-S was separated from bound by alternating centrifugation and washing of the beads in ice-cold binding buffer. The radioactivity associated with the beads was then measured. Binding was expressed as a percentage of the radioactivity associated with wild-type RBD. Experiments with GST but no RBD were performed as controls, to estimate nonspecific binding of Ras. The $K_d$ of the R89K mutant from Ras was determined by Wittinghofer et al. to be greater than 100 at low ionic strength (Block et al., 1996).

*Relation to the standard binding free energy change*

It is worth noting that the choice of units for the measured reduction in binding constant (number density of protein molecules, or equivalently molar concentrations) corresponds to a standard free energy change with the standard state defined by 1 M concentration of ideal solution at room temperature and pressure. This correspondence holds as long as the experimental protein concentrations are low enough to be approximately ideal (Ben Naim, 1973). This is approximately verified here; e.g., the solution concentrations are micromolar, and the surface concentration of protein on the agarose beads is estimated to be on the order of one molecule per $300 \times 300$ Å$^2$ at most. The simulations correspond to the same standard conditions (equal and sufficiently dilute concentrations of reactants and products) (Gilson et al., 1997).

## Computational

*Starting structures of the Ras–RBD complex*

The Ras–RBD complex was built by superimposing the $C_\alpha$ atoms of Ras onto those of Raps in the crystal complex by least-squares fit; the effector domain coordinates (residues 29–42) were then taken explicitly from the Raps–RBD crystal structure; finally, 400 steps of conjugate gradient minimization were done with the CHARMM19 force field, during which the backbone atoms shifted by just 0.32 Å. This model was used as a starting point for molecular dynamics. The Ras–RBD(R89K) complex structure was obtained by placing Lys89 on top of Arg89 in the Ras–RBD structure, followed by 400 steps of conjugate gradient energy minimization.

*Force field and molecular dynamics protocol*

Simulations were done with two different force fields for the protein: the CHARMM19 (Brooks et al., 1983) and the CHARMM22 (Mackerell et al., 1998) force fields. Earlier simulations of the free RBD with the OPLS/AMBER force field (Jorgensen & Tirado-Rives, 1988) are available for comparison. Water molecules were described by a modified TIP3P model (Jorgensen et al., 1983; Neria et al., 1996). Molecular dynamics simulations were carried out with the stochastic boundary method (Brooks & Karplus, 1984; Brooks et al., 1985), including a spherical region centered on the Ala85 carbonyl oxygen, the approximate center of the binding interface. The radius of the sphere was 14 Å for the free RBD simulations and 16 Å for the complex. This region contained about half of the RBD and 238 water molecules, or about half of the Ras–RBD complex and 188 water molecules. Backbone and side-chain groups were not subdivided. To keep the simulation system close to neutral, we deleted the charged portions of the side chains of Arg59, Lys65, and Arg73, which are located near the surface of the spherical region and are unsolvated in the model. The net charge of the system is then + 1 for the RBD and −2 for the complex. Since the R89K mutation preserves the net charge, this difference is not expected to be important. Protein atoms in the outer 2 Å (buffer region) of the simulation zone were restrained by a harmonic force. Constant temperature molecular dynamics simulations were carried out at 25 °C (Berendsen et al., 1984). The internal geometry of water molecules was constrained with the SHAKE algorithm (Ryckaert et al., 1977). Electrostatic interactions were truncated on a group basis at a distance of 13 Å. Simulations were run using the X-PLOR program (Brünger, 1992).

*Alchemical free energy calculations*

The free energy calculations model the alchemical transformation of the native Arg89 into a Lys, either in the free RBD or in the Ras–RBD complex. A hybrid residue 89 is introduced with two side chains, one of each type. Their interactions with their environment are weighted by factors $\lambda$ and $1 - \lambda$, respectively, where $\lambda$ is between 0 and 1. The potential energy has the form

$$U(\lambda) = U^b + U_{11}^{nb} + U_{22}^{nb} + U_{33}^{nb} + (1-\lambda)U_{12}^{nb} + \lambda U_{13}^{nb} + U_{res}, \tag{1}$$

where $U^b$ represents all the bonded interactions in the system; $U_{11}^{nb}$ represents nonbonded interactions outside the hybrid side chain; $U_{ii}^{nb}$, $i = 2,3$, represent nonbonded interactions within the Arg and Lys side-chain moieties, respectively, and $U_{1i}^{nb}$ represents the nonbonded interactions of these moieties with the rest of the system. $U_{res}$ is a restraint term used in the free RBD simulations to maintain the RRH in either its H or T conformation by restraining the interatom distances $r$(O84–H88) and $r$(O85–H89) within the range characteristic of that conformation. It has a flat-bottomed form (Hermans et al., 1992; Zeng et al., 1998) so as to minimize its perturbing effect on the system.

The free energy change due to a small change $\delta\lambda$ in $\lambda$ is (McQuarrie, 1975)

$$\delta G = \frac{dG}{d\lambda}\,\delta\lambda = \left\langle \frac{\partial U}{\partial \lambda} \right\rangle_\lambda \delta\lambda, \tag{2}$$

where the brackets indicate an ensemble average performed at a given value of $\lambda$. The derivative $\langle \partial U/\partial \lambda \rangle_\lambda$ was calculated by molecular dynamics simulations at $\lambda = 0.03, 0.1, 0.3, 0.5, 0.7, 0.9, 0.97$. For the initial windows, at least 70 ps of equilibration and 70 ps of data collection were performed; for subsequent windows, 10 ps of equilibration and 30 ps of data collection. Integration of the free energy derivatives between $\lambda = 0.03$ and 0.97 was done with a trapezoidal method. To correctly account for endpoint singularities, integration from $\lambda = 0$ to 0.03 and from 0.97 to 1 was done by extrapolating the free energy derivative with one of two possible forms. The first is a linear extrapolation based on the first and second derivatives at $\lambda = 0.03$ or 0.97. The second uses a linear extrapolation for the electrostatic term, and for the van der Waals term, the theoretical form of the free energy derivative for particle creation or annihilation in simple van der Waals liquids (Simonson, 1993).

The free energies to apply the restraints (when present) in the first window and to remove them in the last window were small, and could be accurately obtained by

$$\Delta G_{res} = -kT \ln\langle \exp(U_{res}/kT) \rangle, \tag{3}$$

where $k$ is Boltzmann's constant and $T$ the absolute temperature.

*Boltzmann average over the H and T conformations*

In the free RBD, the Arg89 → Lys free energy change must be averaged over the results for the H and T conformations, with Boltzmann weighting:

$$\begin{aligned}
\Delta G_{\mathrm{RBD}}(\mathrm{R} \rightarrow \mathrm{K}) &= -kT \ln Z_{\mathrm{R89K}}/Z_{\mathrm{RBD}} \\
&= -kT \ln \frac{\exp[-G_{\mathrm{R89K}}(\mathrm{T})/kT] + \exp[-G_{\mathrm{R89K}}(\mathrm{H})/kT]}{\exp[-G_{\mathrm{RBD}}(\mathrm{T})/kT] + \exp[-G_{\mathrm{RBD}}(\mathrm{H})/kT]} \\
&= \Delta G_{\mathrm{H}}(\mathrm{R} \rightarrow \mathrm{K}) - kT \ln \frac{1 + \exp[-\Delta G_{\mathrm{R89K}}(\mathrm{H} \rightarrow \mathrm{T})/kT]}{1 + \exp[-\Delta G_{\mathrm{RBD}}(\mathrm{H} \rightarrow \mathrm{T})/kT]}
\end{aligned} \tag{4}$$

where $Z_{\mathrm{R89K}}$ and $Z_{\mathrm{RBD}}$ represent the partition functions of the R89K and native forms of the RBD, respectively, and the notations for the free energies are self-explanatory.

*Free energy component analysis*

Free energy component analysis has been described elsewhere (Gao et al., 1989; Simonson & Brünger, 1992; Boresch et al., 1994; Archontis et al., 1998). An atom $i$ that is not part of the hybrid side chain contributes the terms $U_{i0}(\lambda) + \Sigma_{i<j} U_{ij}$ to the energy function, where $U_{i0}(\lambda)$ is the interaction with the hybrid side chain and $U_{ij}$ represents other interactions. The contribution to the free energy derivative is $\langle \partial U_{i0}/\partial \lambda \rangle_\lambda$; integrating over $\lambda$ gives the direct free energy contribution of atom $i$. Summing over a group of atoms gives the group free energy contribution, or component.

## Acknowledgments

J.Z. gratefully acknowledges a C.J. Martin Fellowship (No. 967362) awarded by the Australian National Health and Medical Research Council. T.S. acknowledges support from the IDRIS Supercomputer Center and from the Simulation Numérique Program of the Centre National de la Recherche Scientifique. We thank Tran Trung Tran for preparing Figure 2.

## References

Archontis G, Karplus M. 1996. Cumulant expansion of the free energy: Application to free energy derivatives and component analysis. *J Chem Phys 105*:11246–11260.

Archontis G, Simonson T, Moras D, Karplus M. 1998. Specific amino acid recognition by aspartyl-tRNA synthetase studied by free energy simulations. *J Mol Biol 275*:823–846.

Ben Naim A. 1973. Standard thermodynamics of transfer. Uses and misuses. *J Phys Chem 82*:792–803.

Berendsen H, Postma J, van Gunsteren W, DiNola A, Haak J. 1984. Molecular dynamics with coupling to an external bath. *J Chem Phys 81*:3684–3690.

Block C, Janknecht R, Herrmann C, Nassar N, Wittinghofer A. 1996. Quantitative structure-activity analysis correlating Ras/Raf interaction in vitro to Raf activation in vivo. *Nat Struct Biol 3*:244–251.

Boresch S, Archontis G, Karplus M. 1994. Free energy simulations: The meaning of the individual contributions from a component analysis. *Proteins 20*:25–33.

Boresch S, Karplus M. 1995. The meaning of component analysis: Decomposition of the free energy in terms of specific interactions. *J Mol Biol 254*:801–807.

Brady G, Szabo A, Sharp K. 1996. On the decomposition of free energies. *J Mol Biol 263*:123–125.

Brooks B, Bruccoleri R, Olafson B, States D, Swaminathan S, Karplus M. 1983. CHARMM: A program for macromolecular energy, minimization, and molecular dynamics calculations. *J Comp Chem 4*:187–217.

Brooks C, Brünger AT, Karplus M. 1985. Active site dynamics in proteins: A stochastic boundary molecular dynamics approach. *Biopolymers 24*:843–865.

Brooks C, Karplus M. 1984. Deformable stochastic boundaries in molecular dynamics. *J Chem Phys 79*:6312–6325.

Brünger AT. 1992. X-plor *version 3.1, A system for X-ray crystallography and NMR*. New Haven: Yale University Press.

deVos A, Tong L, Milburn M, Matias P, Jancarik J, Noguchi S, Nishimura S, Miura K, Ohtsuka E, Kim S. 1988. Three-dimensional structure of an oncogene protein: The catalytic domain of c-H-Ras. *Science 247*:939–945.

Diamond R. 1990. On the use of normal modes in thermal parameter refinement: Theory and application to the bovine pancreatic trypsin inhibitor. *Acta Cryst A46*:425–435.

Emerson SD, Madison VS, Palermo RE, Waugh DS, Scheffler JE, Tsao KL, Kiefer ST, Liu SP, Fry DC. 1995. Solution structure of the Ras-binding domain of c-Raf-1 and identification of its Ras interaction sites. *Biochemistry 30*:6911–6918.

Fabian J, Vojtek A, Cooper J, Morrison D. 1994. A single amino acid change in Raf-1 inhibits Ras binding and alters Raf-1 function. *Proc Natl Acad Sci USA 91*:5982–5986.

Fridman M, Tikoo A, Varga M, Murphy A, Nur-El-Kamal M, Maruta H. 1994. The minimal fragments of c-Raf-1 and NF1 that can suppress v-Ha-Ras-induced malignant phenotype. *J Biol Chem 269*:30105–30108.

Gao J, Kuczera K, Tidor B, Karplus M. 1989. Hidden thermodynamics of mutant proteins: A molecular dynamics analysis. *Science 244*:1069–1072.

Geyer M, Herrmann C, Wohlgemuth S, Wittinghofer A, Kalbitzer HR. 1997. Structure of the Ras-binding domain of RalGEF and implications for Ras binding and signaling. *Nat Struct Biol 4*:694–699.

Gibbs J, Sigal I, Poe M, Scolnic E. 1984. Intrinsic GTPase activity distinguishes normal and oncogenic ras p21 molecules. *Proc Natl Acad Sci USA 81*:5704–5708.

Gilson M, Given J, Bush B, McCammon JA. 1997. The statistical-thermodynamic basis for computation of binding affinities: A critical review. *Biophys J 72*:1047–1069.

Heidecker G, Kolch N, Morrison DK, Rapp UR. 1992. The role of Raf-1 phosphorylation in signal transduction. *Adv Cancer Res 58*:53–73.

Hermans J, Yun RH, Anderson AG. 1992. Precision of free energies calculated by molecular dynamics simulations of peptides in solution. *J Comp Chem 13*:429–442.

Higuchi R, Krummel B, Saiki R. 1988. A general method of in vitro preparation and specific mutagenesis of DNA fragments: Study of protein and DNA interactions. *Nucl Acids Res 16*:7351–7367.

Ho S, Hunt H, Horton R, Pullen J, Pease L. 1989. Site-directed mutagenesis by overlap extension using the polymerase chain reaction. *Gene 77*:51–59.

Hodel A, Rice L, Simonson T, Fox RO, Brünger AT. 1995. Proline cis-trans isomerization in staphylococcal nuclease: Multi-substate free energy perturbation calculations. *Protein Sci 4*:634–654.

Hodel A, Simonson T, Fox RO, Brünger AT. 1993. Conformational substates and uncertainty in macromolecular free energy calculations. *J Phys Chem 97*:3409–3417.

Howlin B, Moss D, Harris G. 1990. Segmented anisotropic refinement of bovine ribonuclease A by the application of the rigid-body TLS model. *Acta Cryst A45*:851–861.

Huang L, Weng X, Hofer F, Martin GS, Kim S. 1997. Three-dimensional structure of the Ras-interacting domain of RalGDS. *Nat Struct Biol 4*:609–615.

Janin J. 1995. Protein–protein recognition. *Prog Biophy Mol Biol 64*:145–166.

Janin J, Miller S, Chothia C. 1988. Surface, subunit interfaces and interior of oligomeric proteins. *J Mol Biol 204*:155–164.

Jones S, Thornton J. 1995. Protein–protein interactions: A review of protein dimer structures. *Prog Biophys Mol Biol 63*:31–65.

Jorgensen W, Tirado-Rives J. 1988. The OPLS potential function for proteins, energy minimization for crystals of cyclic peptides and crambin. *J Am Chem Soc 110*:1657–1666.

Jorgensen WL, Chandrasekar J, Madura J, Impey R, Klein M. 1983. Comparison of simple potential functions for simulating liquid water. *J Chem Phys 79*:926–935.

Kraulis P, Domaille P, Campbell-Burk S, van Aken T, Laue E. 1994. Solution structure and dynamics of ras p21:GDP determined by heteronuclear three- and four-dimensional NMR spectroscopy. *Biochemistry 33*:3515–3531.

Lau F, Karplus M. 1994. Molecular recognition in proteins. Simulation analysis of substrate binding by a tyrosyl-tRNA synthetase mutant. *J Mol Biol 87*:1049–1066.

Mackerell A, Bashford D, Bellott M, Dunbrack R, Evanseck J, Field M, Fischer S, Gao J, Guo H, Ha S, Joseph D, Kuchnir L, Kuczera K, Lau F, Mattos C, Michnick S, Ngo T, Nguyen D, Prodhom B, Reiher W, Roux B, Smith J, Stote R, Straub J, Watanabe M, Wiorkiewicz-Kuczera J, Yin D, Karplus M. 1998. An all-atom empirical potential for molecular modelling and dynamics study of proteins. *J Phys Chem B 102*:3586–3616.

Mackerell A, Wiorkiewicz-Kuczera J, Karplus M. 1995. An all-atom empirical energy force-field for the study of nucleic acids. *J Am Chem Soc 117*:11946–11975.

Mark AE, Gunsteren WFV. 1994. Decomposition of the free energy of a system in terms of specific interactions. *J Mol Biol 240*:167–176.

Maruta H, Holden J, Sizeland A, D'Abaco G. 1991. The residues of Ras and Rap proteins that determine their GAP specificities. *J Biol Chem 266*:11661–11668.

McCormick F, Wittinghofer A. 1996. Interactions between Ras proteins and their effectors. *Curr Opin Biotech 7*:449–456.

McQuarrie D. 1975. *Statistical mechanics*. New York: Harper and Row.

Miyamoto S, Kollman PA. 1993. Absolute and relative binding free energy calculations of the interaction of biotin and its analogs with streptavidin using molecular dynamics/free energy perturbation approaches. *Proteins 16*:226–245.

Moodie SA, Willumsen BM, Weber MJ, Wolfman A. 1993. Complexes of Ras-GTP with Raf-1 and mitogen-activated protein kinase kinase. *Science 260*:1658–1661.

Nassar N, Horn G, Herrmann C, Block C, Janknecht R, Wittinghofer A. 1996. Ras/Rap effector specificity determined by charge reversal. *Nat Struct Biol 3*:723–729.

Nassar N, Horn G, Herrmann C, Scherer A, McCormick F, Wittinghofer, A. 1995. The 2.2 Å crystal structure of the Ras-binding domain of the serine/threonine kinase c-Raf-1 in complex with Rap1A and a GTP analogue. *Nature 375*:554–560.

Neria E, Fischer S, Karplus M. 1996. Simulation of activation free energies in molecular systems. *J Chem Phys 105*:1902–1921.

Nina M, Beglov D, Roux B. 1997. Atomic radii for continuum electrostatics calculations based on molecular dynamics free energy simulations. *J Phys Chem 101*:5239–5248.

Pai E, Kabsch W, Krengel U, Holmes K, John J, Wittinghofer A. 1989. Structure of the guanine-nucleotide-binding domain of the Ha-Ras oncogene product p21 in the triphosphate conformation. *Nature 341*:209–214.

Pomes R, Wilson R, McCammon JA. 1995. Free energy simulations of the HyHEL-10/HEL antibody–antigen complex. *Protein Eng 8*:663–675.

Resat H, Mezei M. 1994. Studies on free energy calculations. II. A theoretical approach to molecular solvation. *J Chem Phys 222*:6126–6140.

Ryckaert J, Ciccotti G, Berendsen H. 1977. Numerical integration of the Cartesian equations of motion for a system with constraints. *J Comput Phys 23*:327–341.

Shirouzu M, Koide H, Fuita-Yoshigaki J, Oshio H, Toyama Y, Yamasaki K, Fuhrman SA, Villafranca E, Kaziro Y, Yokovama S. 1994. Mutations that abolish the ability of Ha-Ras to associate with Raf-1. *Oncogene 9*:2153–2157.

Simonson T. 1993. Free energy of particle insertion. An exact analysis of the origin singularity for simple liquids. *Mol Phys 80*:441–447.

Simonson T, Brünger AT. 1992. Thermodynamics of protein–peptide binding in the ribonuclease S system studied by molecular dynamics and free energy calculations. *Biochemistry 31*:8661–8674.

Sternberg M, Grace D, Phillips D. 1979. Dynamic information from protein crystallography. *J Mol Biol 130*:231–253.

Sun Y, Veenstra D, Kollman P. 1996. Free energy calculations of the mutation of Ile96 → Ala in barnase: Contributions to the difference in stability. *Prot Eng 9*:273–281.

Tobias DJ, Brooks CL, Fleischman SH. 1989. Conformational flexibility in free energy simulations. *Chem Phys Lett 156*:256–260.

van Gunsteren W, Weiner P, eds. 1989. *Computation of free energy for biomolecular systems*. Leiden: Escom Science Publishers.

Vojtek AB, Hollenberg SM, Cooper JA. 1993. Mammalian Ras interacts directly with the serine/threonine kinase Raf. *Cell 74*:205–214.

Wade R, McCammon JA. 1992. Binding of an antiviral agent to a sensitive and a resistant human rhinovirus. Computer simulation studies with sampling of amino acid side chain conformations. *J Mol Biol 225*:679–712.

Weiner S, Kollman P, Case D, Singh U, Ghio C, Alagona G, Profeta S, Weiner P. 1984. A new force field for molecular mechanical simulation of nucleic acids and proteins. *J Am Chem Soc 106*:765–784.

Zeng J, Treutlein HR, Simonson T. 1998. The conformation of the Ras-binding domain of Raf studied by molecular dynamics and free energy simulations. *Proteins 31*:186–200.

Zeng J, Treutlein HR, Simonson T. 1999. Molecular dynamics simulations of the Ras:Raf and Ras:Rap complexes. *Proteins*. In press.

Zhang XF, Settleman J, Kyriakis JM, Takeuchi-Suzuki E, Elledge SJ, Marshall MS, Bruder JT, Rapp UR, Avruch J. 1993. Normal and oncogenic $p21^{Ras}$ proteins bind to the amino-terminal regulatory domain of c-Raf-1. *Nature 364*:308–313.